Charge Transport in High-Mobility Field-Effect Transistors Based on Inkjet Printed Random Networks of Polymer Wrapped Single-Walled Carbon Nanotubes

Scuratti, Francesca; Salazar-Rios, Jorge Mario; Luzio, Alessandro; Kowalski, Sebastian; Allard, Sybille; Jung, Stefan; Scherf, Ullrich; Loi, Maria Antonietta; Caironi, Mario

Published in:
Advanced Functional Materials

DOI:
10.1002/adfm.202006895

ADVANCED FUNCTIONAL MATERIALS
www.afm-journal.de

Charge Transport in High-Mobility Field-Effect Transistors Based on Inkjet Printed Random Networks of Polymer Wrapped Single-Walled Carbon Nanotubes

*Francesca Scuratti, Jorge Mario Salazar-Rios, Alessandro Luzio, Sebastian Kowalski, Sybille Allard, Stefan Jung, Ullrich Scherf, Maria Antonietta Loi, and Mario Caironi**

Printed random networks of polymer-wrapped multi-chiral semiconducting carbon nanotubes (s-SWCNTs) are an opportunity for mass-manufacturable, high-performance large-area electronics. To meet this goal, a deeper understanding of charge-transport mechanisms in such mixed networks is crucial. Here, charge transport in field-effect transistors based on inkjet-printed s-SWCNTs networks is investigated, obtaining direct evidence for the phases probed by charge in the accumulated channel, which is critical information to rationalize the different transport properties obtained for different printing conditions. In particular, when the fraction of nanotubes with smaller bandgaps is efficiently interconnected, the sparse network provides efficient charge percolation for band-like transport, with a charge mobility as high as 20.2 $cm^2 V^{-1} s^{-1}$. However, when the charges are forced by a less efficient morphology, to populate also higher bandgap nanotubes and and/or the wrapping polymer, thermally activated transport takes place and mobility drops. As a result, a trade-off between network density and charge transport properties is identified for device current optimization, in both p- and n-type regimes. These findings shed light on the fundamental aspects related to charge transport in printed s-SWCNT mixed networks and contribute to devise appropriate strategies for the formulation of inks and processes towards cost-effective mass production schemes of high-performance large-area electronics.

1. Introduction

Semiconducting single-walled carbon nanotubes (s-SWCNT) are currently object of intensive research thanks to their impressive mechanical and electronic properties[1–4] that, along with their processability from solution at low temperature, make them ideal candidates for high-performance printed and flexible large-area electronics.[5]

Since the growth process of carbon nanotubes always produces mixtures of metallic and semiconducting chiralities, it is necessary to separate them before further processing. Among other approaches, noncovalent functionalization of the sidewalls through polymeric chains, that is, polymer wrapping, has emerged as a very effective technique for the high-yield sorting of s-SWCNTs with purities >99.9% and the production of stable dispersions suitable for inks formulation.[6–11]

The possibility to manage and deposit s-SWCNTs from solution at low temperature and ambient pressure conditions is particularly appealing in view of achieving a large-scale production, based on cost-effective methods for large area deposition on flexible substrates, as offered by printing technologies.[12] Indeed, field-effect transistors (FETs) based on networks of polymer-wrapped s-SWCNTs with mobility higher than 10 $cm^2 V^{-1} s^{-1}$ and on-off current ratios up to 10^8 have been successfully demonstrated by using doctor blading and inkjet printing.[13,14]

However, the full potential of carbon nanotubes in printed electronics applications is still hindered by a general lack of understanding of charge transport mechanisms in mixed networks: the influence of the presence of a distribution of

Dr. F. Scuratti, Dr. A. Luzio, Dr. M. Caironi
Center for Nano Science and Technology @PoliMi
Istituto Italiano di Tecnologia
Via Pascoli 70/3, Milan 20133, Italy
E-mail: mario.caironi@iit.it

The ORCID identification number(s) for the author(s) of this article can be found under https://doi.org/10.1002/adfm.202006895.

[+]Present address: Universidad de Manizales, Cra. 9a # 19-03, Manizales, Caldas 170001, Colombia

DOI: 10.1002/adfm.202006895

Dr. F. Scuratti
Department of Electronics
Information and Bioengineering
Politecnico di Milano
Piazza Leonardo Da Vinci 32, Milan 20133, Italy
Dr. J. M. Salazar-Rios[+], Prof. M. A. Loi
Zernike Institute for Advanced Materials
University of Groningen
Nijenborgh, Groningen, AG 4 9747, The Netherlands
Dr. S. Kowalski, Dr. S. Allard, Dr. S. Jung, Prof. U. Scherf
Macromolecular Chemistry and Center for Smart Materials and Systems
University of Wuppertal
Gauss-Str. 20, D-42119 Wuppertal, Germany

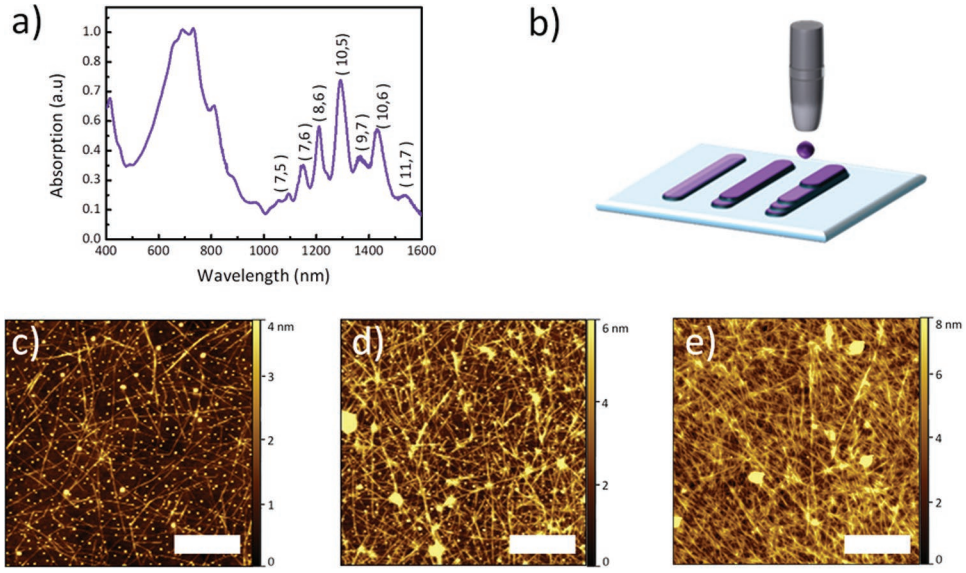

Figure 1. a) Absorption spectrum of the HiPCO:P12CPDTBT ink used in this work. The chiralities of the SWCNTs present in the dispersion are determined using an empirical equation.[28,29] b) Sketch of the inkjet printing process adopted for the deposition of multiple printing passes of the s-SWCNTs solution with a nozzle orifice diameter of 60 µm. The drop spacing was set at 100 µm and the printing speed was 50 mm s^{-1}. c–e) AFM topography maps of the s-SWCNTs networks obtained by c) one, d) three, and e) ten printing passes. Scale bars are 500 nm.

semiconducting chiralities and diameters on the network transport efficiency, as well as the impact of the network morphology and density, and the role of the functionalizing polymer are in fact still unclear. Thus, a thorough rationalization of the factors determining charge transport properties in these systems is highly desirable to rationally tailor and guide their processing, in view of drastically improving the performances of printed carbon nanotube based FETs.

Several works already highlighted the importance of identifying how the distribution of the different energy levels and bandgaps affects charge transport in solution-processed random networks. Temperature-dependent mobility measurements on dense s-SWCNT networks have shown thermally activated transport that can be fitted with a fluctuation induced tunneling (FIT) model,[15–17] and the analysis carried out by Rother et al. on networks with varying compositions suggested that narrow distributions of large-diameter tubes are better suited to achieve optimal transporting conditions in a mixed network.[15,18] The latter conclusion was further corroborated through direct evidence gathered via charge-modulated absorption and photoluminescence spectroscopy in a recent study by Zorn et al.[19]

The influence of the wrapping polymer on transport has also been subject of investigation.[15,20] Several efforts have been made either in the direction of understanding which polymers are best suited to affect as little as possible charge transport, or towards removing the wrapping polymer altogether in post processing.[21–24] However a direct evidence of the involvement of the polymer in charge transport in FETs has not been reported yet.

In addition, the adoption of solution-based deposition methods poses the question on the best processing conditions for achieving optimum network parameters, for example, whether it exists a more favorable network morphology or spatial density/thickness that maximizes transport efficiency and thus device performance.

In this work, we carry out an extensive investigation of charge transport properties in polymer-wrapped mixed carbon nanotube networks with variable spatial density and thickness, deposited by inkjet printing. The network density was controlled by performing multiple printing passes. This allowed to tune the charge transport in transistors, which spans from a balanced ambipolar behavior, for low network densities, to a prevalent p-type behavior, for high density films. Importantly, we observed a different temperature dependence of mobility with variable printing passes, ranging from a thermally activated to a "band-like" (i.e., characterized by inverted thermal activation) transport, thus denoting a non-trivial interplay between channel coverage and charge transport properties for holes and electrons. We adopted charge modulation spectroscopy (CMS) to rationalize such observations. Sparse networks are characterized by selective charge population in favor of smaller energy bandgaps nanotubes, with substantially no signature of the polymer. Instead, denser networks display increased involvement of higher bandgap nanotubes, introducing energetic barriers to transport. Remarkably, we also observe unambiguous charge relaxation over the polymer, further contributing to limit transport properties in higher coverage devices. Such mutual interplay of network density and morphology, distribution of s-SWCNTs chiralities and wrapping polymer, is key to maximize the printed FETs currents, as it introduces a trade-off between channel coverage and charge mobility.

2. Results

In this work, we used poly[4,4-didodecyl-4*H*-cyclopenta[2,1-b:3,4-b']-dithiophene-2,6-diyl)-alt-(2,1,3-benzothiadiazole-4,7-diyl)] (P12CPDTBT)[25–27] for the high-yield sorting of semiconducting chiralities of high-pressure carbon monoxide (HiPCO)

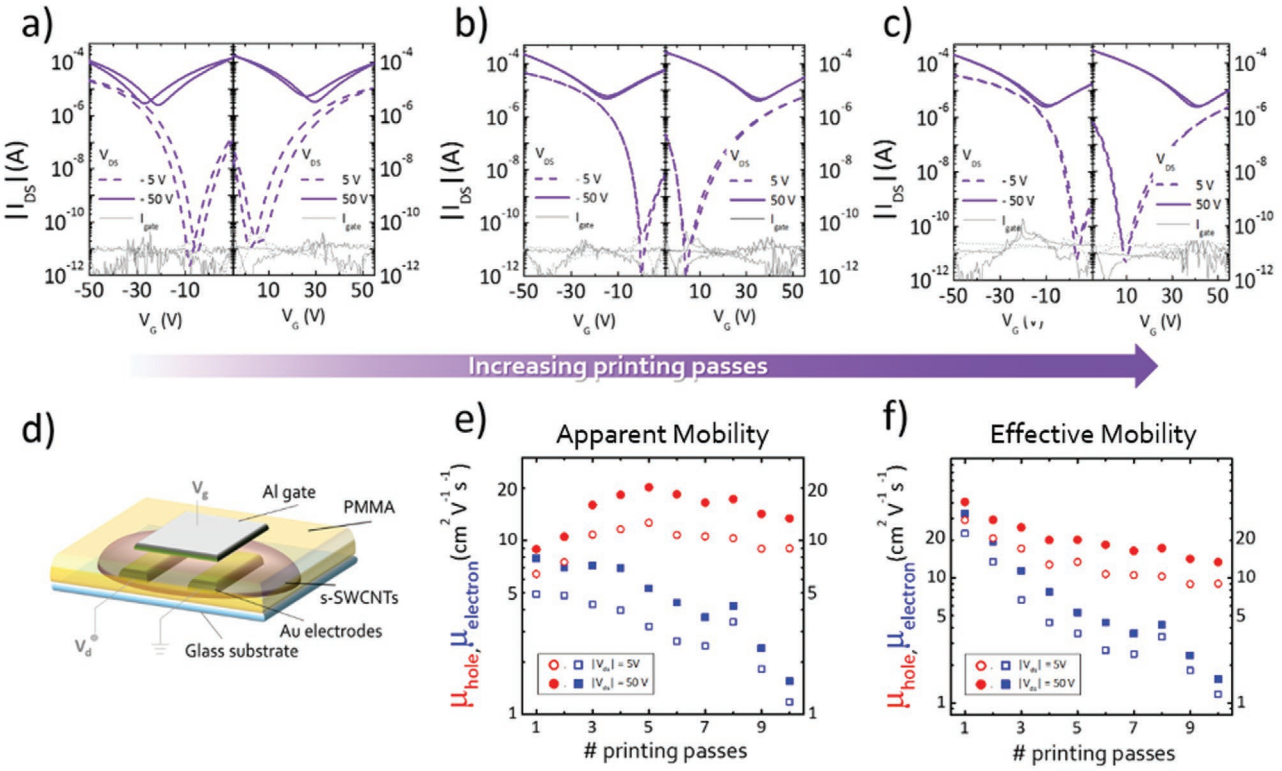

Figure 2. a–c) Transfer characteristics of HiPCO:P12CPDTBT based FETs, made with increasing printing passes, respectively a) one, b) five, and c) ten. d) Sketch of the top gate-bottom contact architecture adopted for the SWCNTs-based FETs. Channel width W = 200 µm, channel length L = 40 µm. e) Apparent mobility data values as a function of the number of printing passes, extracted at $|V_g|$ = 50 V. The hole (red circles) and electron (blue squares) mobility in linear ($|V_{ds}|$ = 5 V, empty symbols) and saturation ($|V_{ds}|$ = 50 V, filled symbols) are reported. f) Effective mobility plot of the FETs. Effective mobility is determined by rescaling apparent mobility for the network coverage, as extracted from AFM images.

synthesized SWCNTs.[23] The P12CPDTBT wrapped SWCNTs were first dispersed in toluene, selecting tubes with diameters between 0.8 and 1.2 nm. The formulation was then redispersed in ortho-dichlorobenzene (oDCB), a solvent more suitable for inkjet printing carbon based materials due to its higher boiling point, which was also successfully adopted in the past for the inkjet printing of carbon nanotube networks in high-performance FETs.[14] The absorption spectrum of the resulting ink is shown in **Figure 1**a. The peaks centered around 400 and 700 nm correspond to the polymer absorption and, since the solution was purified and enriched, these peaks are mostly due to polymer chains wrapping the SWCNTs. The sharp peaks in the infrared region are the absorption transitions E_{11} from the different SWCNT chiralities, assigned according to an empirical formula.[23]

The adoption of oDCB as a solvent for the s-SWCNT-based ink granted the achievement of stable and controlled jetting conditions, allowing the multi-layer printing of uniform and interconnected networks. Networks of P12CPDTBT wrapped s-SWCNTs with different spatial density were thus realized by varying the number of inkjet printing passes, from one to ten (Figure 1b). Atomic force microscopy pictures in Figure 1c–e, performed into the channel of the FETs realized for the electrical characterizations, show the topographical features of the networks and their evolution with increasing printed layers.

Starting from a sparse but well interconnected network with a total channel coverage of ≈22% for a single printing pass (Figure 1c), the network density gradually increases (in Figure 1d the topography of the three printing passes film is shown) until it reaches complete coverage around the fifth printed layer (Section S1.1, Supporting Information). If more ink is added, the s-SWCNTs start to stratify uniformly with no further variations in the total coverage, thus contributing only to the overall thickness of the deposited network (Figure 1e).

The electrical properties of the printed networks were investigated in a top gate, bottom contact FET architecture (**Figure 2**d). The networks were deposited by inkjet printing in air and at room temperature on source and drain gold contacts patterned by a lithographic lift-off process, and were subsequently coated with a polymethyl methacrylate (PMMA) dielectric, on top of which an Al gate electrode was evaporated. For the detailed fabrication process we refer the reader to the Section 5.

Typical transfer characteristics of the printed HiPCO:P12CPDTBT based FETs are reported in Figure 2a–c. For a single printing pass, in spite of the low network coverage, the devices already show excellent characteristics, featuring a clean and balanced ambipolar behavior in saturation ($|V_{ds}|$ = 50 V) with high on-off ratios (calculated at $|V_{ds}|$ = 5 V and $|V_g|$ = 50 V) between 10^6 and 10^7 (Figure 2a), as a result of the excellent selectivity of the wrapping polymer towards semiconducting SWCNT chiralities only. By incrementing the number of

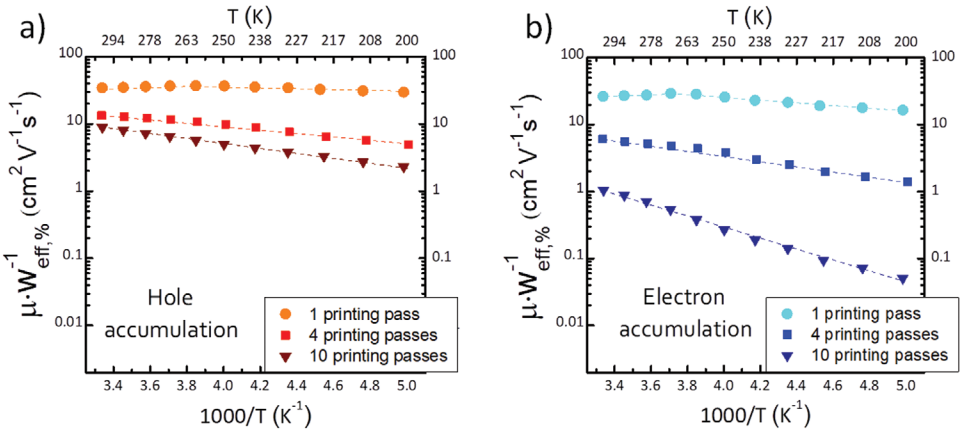

Figure 3. a–b) Temperature dependent effective mobility data extracted from the saturation regime ($|V_{ds}| = 40$ V, $|V_g| = 50$ V) for a) holes and b) electrons for samples made with one (circles), four (squares) and ten (triangles) printing passes. The values reported, already rescaled for the effective channel width, were extracted at the same voltage overdrive, thus taking into account any temperature dependent threshold voltage shifts.

printing passes, the I_{ds} currents for the p-type channel increase as expected from the higher network density, which allows more percolation paths to be available; quite interestingly, an opposite trend of weakly reducing currents with coverage can be noted for the n-type channel (Figure 2b), thus leading to a more unbalanced ambipolarity.

After the completion of the network in terms of surface coverage (corresponding to the fifth printing pass), when more material is added a deterioration of the performances is generally observed, as the currents measured both in hole and in electron accumulation decrease. Such reduction is stronger for the currents in the n-type accumulation regime, which drop by more than one order of magnitude for the ten printing passes device, when compared to the single printing pass one (Figure 2c). As a result, the devices realized with ten printing passes display a predominantly p-type transport.

The peculiar trend highlighted for the FETs currents is obviously reflected also in the apparent field effect mobility values of the devices, that is, estimated without considering the channel coverage, as a function of the number of printing passes. The mobility data, extracted at $|V_g| = 50$ V using the gradual channel approximation model, are reported in Figure 2e both for the linear (empty symbols) and the saturation (filled symbols) regimes. The single printing pass device exhibits balanced hole ($\mu_{lin,hole}$) and electron ($\mu_{lin,electron}$) linear apparent mobility of 6.4 and 4.9 $cm^2\ V^{-1}\ s^{-1}$, and saturation apparent mobility for holes ($\mu_{sat,hole}$) and electrons ($\mu_{sat,electron}$) of 8.9 and 7.9 $cm^2\ V^{-1}\ s^{-1}$. The hole mobility then gradually increases up to a remarkable maximum value of $\mu s_{at,hole} = 20.2\ cm^2\ V^{-1}\ s^{-1}$, reached for the five printing passes device, while the electron mobility deteriorates as more printed layers are added. The measurement reliability factors of mobility, *r*, calculated as suggested by Choi et al.,[30] are reported in Section S2, Supporting Information.

The significant difference in total coverage of the SWCNTs networks according to the number of printing passes is expected to play an obvious role in sizing the device currents, since it is affecting the geometric area of the FETs channels. This implies that the apparent mobility data values should be corrected by the coverage, obtaining what we will refer to as the effective mobility. By renormalizing the mobility trend to the SWCNTs network coverage, it is clear that the decrease in transport efficiency starts from the very first printing pass (Figure 2f). As a matter of fact, the observed trend in the apparent mobility is the result of the balance between transport properties and available charge paths across the network (increasing with more printing passes). For holes, such balance results in a peak of the apparent mobility (i.e., of the device currents) upon completion of the network (coverage between 95% and 100%). Conversely, for electrons, a more severe loss in transport efficiency occurs with increasing printing passes, and therefore no gain in currents from the enhancement of percolation pathways can be obtained. The origin of the deterioration in transport efficiency can be either related to a worsening of the injection mechanism from the electrodes with denser networks or to the introduction of trap states and barriers hindering charge transport in the accumulated channel of the FET.

We excluded charge injection to be a significant limiting factor, since for all the devices the contact resistance R_c (extracted with the G-function method[31]) is always lower than ≈10% of the channel resistance R_{Ch} (Figure S3.1, Supporting Information), thus indicating that the lowering in mobility with increasing printing passes is not determined by a change in contact resistance.

In order to get insights on the transport mechanism, devices have been characterized by temperature-dependent electrical measurements in the range from 200 to 300 K. Three FETs with different coverage were characterized, choosing a low, an intermediate and a high coverage device as obtained with one, four, and ten printing passes, respectively. The temperature dependences of the effective (i.e., corrected by the coverage) saturation mobility, are reported in **Figure 3** (uncorrected, apparent mobilities both in linear and saturation regimes versus temperature are reported in Figure S4.1, Supporting Information). For all devices characterized, also in this case we carefully assessed contact resistance variations. We verified that R_c variations with temperature are comparable to the variations in R_{Ch}, which also at $T = 200$ K contributes by more than 85% to the total resistance, thus allowing us to exclude variations in effective mobility induced by modifications in injection efficiency (Figure S4.3, Supporting Information).

The ten printing passes network, which corresponds to the worst conditions in terms of mobility for both type of carriers, displays the strongest thermally activated transport in the whole explored range. The corresponding activation energies, extracted using an Arrhenius model, are 75.0 ± 1.5 meV for holes ($E_{act,holes}$) and 143.7 ± 2.9 meV for electrons ($E_{act,electrons}$). For samples with less printing passes, the temperature dependence of transport in the network gradually reduces. Activation energies are already more than halved for the network with four printing passes ($E_{act,holes}$ = 36.3 ± 1.8 meV, $E_{act,electrons}$ = 60.0 ± 1.8 meV).

Interestingly enough, the carrier transport in the single printing pass sample of HiPCO:P12CPDTBT is substantially different from the previous cases, as it does not depend anymore as strongly on temperature. Mobility increases slightly in the 200–260 K region, with $E_{act,holes}$ = 19.3 ± 0.9 meV and $E_{act,electrons}$ = 41.2 ± 2.1 meV. Above 260 K, mobility inverts the trend, displaying a very weak decrease with increasing temperature, a fingerprint of "band-like" transport. This is what would be expected in a pure and highly performing s-SWCNT network, as well as for any high-mobility system, in which hopping theoretically is no longer limiting transport.[32]

Temperature dependent data indicates that low coverage networks feature the most ideal charge transport conditions, as evidenced also by the higher FETs effective mobilities. By enhancing network density through multiple printing passes, thermal activation of transport becomes predominat also close to room temperature, indicating that higher energetic barriers are introduced in the accumulation layer. Such barriers affect more heavily electrons, causing a remarkably different transport efficiency for positive and negative carriers.

We replicated the same analysis with another formulation of HiPCO s-SWCNTs wrapped with a different polymer, the well studied poly(3-dodecylthiophene-2,5-diyl) (P3DDT), which has been widely employed in the past for the fabrication of carbon nanotube-based FETs.[13,14,33] Data from such experiments is included in the Supporting Information (Section S6, Supporting Information). The currents and the mobility of these devices show dependencies with the number of printing passes similar to those observed with the HiPCO:P12CPDTBT formulation, in agreement with the results reported by Bucella et al.[14] Moreover, our temperature-dependent electrical characterizations on HiPCO:P3DDT networks highlighted an enhanced thermal dependence of transport with increasing printing passes, resembling the trends obtained for HiPCO:P12CPDTBT networks . Even though in P3DDT-based devices no clear band-like regime could be reached for the low coverage networks, with an activation energy that tends to vanish close to room temperature, these findings suggest that the observed phenomena are not restricted to the specific wrapping polymer/formulation analyzed.

In order to get deeper insights on such network-dependent transport properties, we carried out charge modulation spectroscopy measurements (CMS). By modulating the gate voltage of an operating FET around a fixed offset bias (V_{os}), CMS probes the variation of a semiconductor optical transmission (ΔT), normalized to the total trasmission (T), induced by charges accumulated at the interface with the dielectric layer. Since it is a modulated spectroscopy technique, CMS can only record spectral features induced by mobile carriers and not by deeply trapped ones, thus giving insights on the species that actually contribute to charge transport. A positive CMS signal ($\Delta T/T > 0$) indicates an increase of the transmitted light and is associated with the bleaching of the ground-state absorption owing to the presence of charges, while a negative CMS signal ($\Delta T/T < 0$) indicates a reduction of transmitted light due to charge-induced absorption.[34]

We specifically investigated a device with strong thermal activation (ten printing passes) and a network showing band-like behavior and more ideal charge transport conditions (one printing pass). CMS spectra for hole and electron accumulation (gate offset voltage $|V_{os}|$ = 40 V, peak-to-peak voltage modulation V_{pp} = 40) are shown in **Figure 4**a,b, respectively. In Figure 4c the optical absorption spectra of the dispersion as a reference is also shown.

Focusing first on the dense network featuring a thermally activated transport (Figure 4a,b dark red and blue solid lines), in the 1100–1600 nm region features with positive $\Delta T/T$ signals for both p-type and n-type accumulation are present, associated to the charge-induced bleaching of the E_{11} transitions of chiralities present in the mixed network. The relative intensities of the peaks match with those in the absorption spectra (see Figure S5.1, Supporting Information), indicating that charges equally probe the SWCNTs distribution in the network, without evident selectivity. In the visible region, for holes accumulation, a bleaching feature between 600 and 800 nm can be observed, followed by a broad charge-induced absorption band extending from 800 to 1100 nm. The bleaching band in the visible range corresponds to the UV–vis absorption spectrum of the wrapping polymer. Therefore we prove that in our networks holes relax on P12CPDTBT, which therefore contributes to charge transport. Consequently, we assign the absorption band at lower energies to the introduction of charged polaronic states in the polymer. The different nature of the CMS signals in the visible and NIR regions is evidenced by their distinct gate-voltage dependence (Figure S5.2, Supporting Information). The NIR peaks assigned to the SWCNTs E_{11} absorption bleaching increase in intensity for low gate offset bias and subsequently decrease when $|V_{os}|$ is raised over 30 V, in agreement with the trends reported in the CMS spectra of s-SWCNTs networks in Ref. [19]. Conversely, the bleaching peak in the visible and its related absorption band increase in magnitude with the gate bias and saturate for high $|V_{os}|$, as typically observed in the charge-modulated absorption spectra of polymers.[34,36] Interestingly, such polymer-related features are completely absent for spectra collected in electron accumulation, which display only weak positive $\Delta T/T$ peaks corresponding to bleaching of E_{22} transitions (detectable also in hole accumulation spectra, superimposed to the polymer signal). This suggests that transport does not involve mobile electrons relaxing on the polymer, either because electrons injected in P12CPDTBT are trapped (and therefore cannot be modulated and detected in a CMS experiment) or cannot be injected at all in the LUMO of the polymer, that nominally lies ≈1.6 eV above the Au Fermi level and ≈0.5 eV above the conduction band SWCNTs with the smallest energy gap (Figure 4d).

A quite distinct landscape emerges for the single printing pass device that features a weak temperature dependence. Indeed, in hole accumulation the P12CPDTBT related CMS

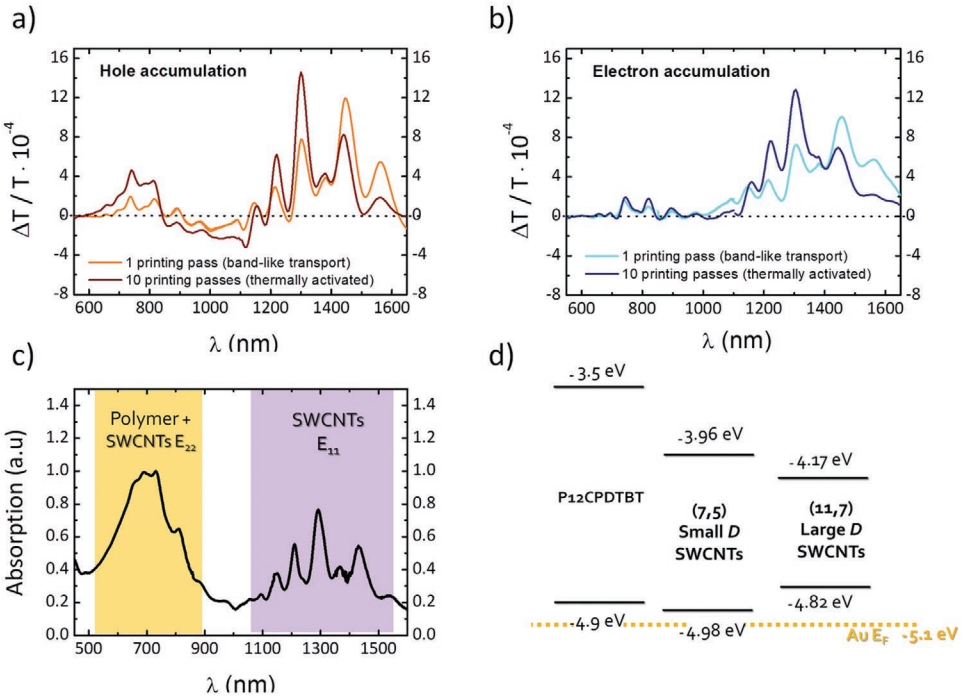

Figure 4. a–b) CMS measurements of polymer wrapped s-SWCNTs based FETs. Gate offset bias is $|V_{os}| = 40$ V, peak-to peak modulation is $V_{pp} = 40$ V. a) CMS spectra in hole accumulation for samples showing band-like (orange) and thermally activated (red) transport. b) CMS in electron accumulation for a band-like (cyan) and a thermally activated (blue) device. c) Absorption spectrum of the HiPCO:P12CPDTBT solution. The regions corresponding to the absorption features of the SWCNTs and of the polymer are highlighted. d) Sketch of the nominal frontier energy levels of the nanotubes-polymer system.[23,35]

signals are much feebler, suggesting that the wrapping polymer is less involved in charge transport; in the case of electrons, these features are identical to the ten passes case. In addition, in both accumulation regimes, the relative intensities of the nanotubes bleaching peaks are rearranged when compared to the absorption spectra of HiPCO:P12CPDTBT and to the charge-modulated spectra of the ten printing passes device (Figure S5.1, Supporting Information): a larger contribution is given by small bandgap chiralities, thus implying that they constitute a preferential charge pathway in low coverage networks. Such a behavior has been detected similarly for different device operational bias, thus excluding possible influences of the gate voltage (Figure S5.2, Supporting Information). Furthermore, any possible artifact induced by Stark effects was excluded via second-harmonic measurements,[19,34,37] which revealed a negligible contribution of electro-absorption in our spectra.

3. Discussion

The analysis of the CMS data gathered in devices with different transport efficiency allow us to propose a picture for the evolution of the transport mechanism in networks with different spatial density.

Previous works demonstrated that in mixed networks charges are preferentially accumulated and transported in small gap tubes.[18,19] Such selectivity is directly evidenced by our CMS data for low coverage samples, where a sparse network, with topographically more clearly discernable nanotubes, is formed. Both carriers tend to populate the lowest energy gap phase, therefore the larger diameter SWCNTs within the distribution, as evidenced by a stronger relative intensity of E_{11} bleaching at lower energies, and almost no involvement of the polymer. From our observations, such phase is characterized by a sufficient interconnectivity not to represent a trap within higher energy gap phases (nominal frontier energetic levels are sketched in Figure 4d). It provides an efficient percolation path from source to drain, along which carriers do not have to overcome large energectic barriers, as those at the interface with the polymer or smaller diameter SWCNTs. Consequently, transport results substantially independent from temperature close to room temperature, a signature of the onset of a band-like behavior, and charge mobility is high, since charge transfer between carbon nanotubes with similar diameter is more efficient, regardless the presence of a spatially thin (few Å) external barrier (e.g., a strand of wrapping polymer).[38,39]

When the coverage increases with printing passes, transistor currents in hole accumulation mode initially evolve accordingly, reflecting the improvement of network interconnectivity, with p-type currents increasing up to the achievement of full network coverage. On the other hand, electron currents are less affected by the enhancement of charge paths and remain unchanged as the number of printed layers is increased from one to four. The advantage deriving from a higher coverage is readily lost after the fifth printed layer, and a pronounced decrease of hole and electron currents is subsequently observed. These effects result from a deterioration of mobility for both carriers, especially for electrons. Such deterioration is correlated to a thermal activated

mobility, with an activation energy markedly higher for electrons and increasing with the number of printing passes. Moreover, CMS data reveal the involvement of a higher fraction of smaller CNTs diameters in transport, and also of the polymer phase in case of holes. Therefore, the additional charge transport paths that become available with more printing passes are clearly not as efficient as those present in the lowest coverage device. Topographies of the printed networks obtained by AFM (Figure 1c–e) become generally less defined, moving from a 2D distribution to a 3D structure, displaying co-presence of larger agglomerates and more intricate and blurred nanotube-like features. The latter results in an increased film roughness (RMS roughness increases from 1.4 nm for the five printing passes device to 2 nm for the ten printing passes device). We can speculate that such intricate morphology can include areas where locally there is not an equal distribution of all the components, with possible presence of a higher fraction of smaller bandgap tubes or even of unwrapped polymer. Consequently, with more printing passes, the availability of percolation paths including only small bandgap tubes, in which transport would preferentially occur, is reduced and charges are forced to exploit also larger gap SWCNTs and polymer segments, as demonstrated by the CMS data. Within such scenario, the misalignment of energy levels introduces an additional energetic cost for both kinds of charge carriers, with the consequent onset of thermal activated transport. In particular, the contribution of the polymer to transport in higher coverage networks is different for electrons and holes. Electron transport is more severely affected, because electrons cannot be injected in the LUMO of the polymer since the SWCNT-polymer energetic barrier is too high (>0.5 eV, Figure 4d), and consequently the possibility of finding percolation paths between source and drain that do not involve the polymer is smaller, more strongly reducing in turn the n-type effective mobility of devices with thicker printed networks. On the other hand, holes can be more easily injected also in the polymer due to the more favorable alignment of the energetic levels. Therefore their transport is less hindered, while obviously suffering the reduced interconnection between nanotubes with similar E_g as well as the less efficient conduction in the polymeric segments. Further studies will be required to clarify the complex morphology of the high coverage samples and further clarify the correlation with the transport properties. However the combination of field-effect mobility, transport temperature dependence and CMS data clearly outline a picture where percolation paths with different transport efficiency are established as printed active layers based on the same formulation of multi-chiral polymer wrapped SWCNTs evolve from a sparse, mostly 2D network with clearly discernible nanotubes to a more dense layer with 3D structuring.

4. Conclusions

In summary, through the controlled deposition of polymer-sorted, P12CPDTBT wrapped SWCNTs networks with variable density by inkjet printing, we realized high-performance balanced ambipolar FETs with saturation mobilities of 8.9 and 7.9 $cm^2\ V^{-1}\ s^{-1}$, for holes and electrons, respectively, as well as mostly unipolar p-type FETs with maximum saturation mobility as high as 20.2 $cm^2\ V^{-1}\ s^{-1}$. In sight of their potential use in future large-area electronic applications, we have then investigated their charge transport properties to understand the role played by the distribution of energy bandgaps, the network density, and the wrapping polymer in sizing the FETs performances.

The device currents and mobility trends showed a dependence on the number of printing passes performed, highlighting the existence of a trade-off between transport efficiency, which is higher in low SWCNTs coverage samples, and available charge paths across the network, that is, network spatial density. Indeed, temperature-dependent measurements evidenced an enhancement of barriers hindering charge transport, especially for electrons, upon increase of the number of printing passes, leading to higher thermal activation energies with respect to a band-like behavior of sparse networks. Charge modulation spectroscopy measurements provide direct evidence that in low density networks the nanotubes with low bandgaps are preferentially more involved in transport. In higher density networks the charge paths reconfigure on all chiralities, reflecting the entire distribution without an evident selectivity, thus bearing an increased contribution from higher bandgap nanotubes for both carriers, and the contribution of the polymer in the case of holes. We attribute such effects, observed for two different high-performance formulations of SWCNT characterized by a different wrapping polymer, to a combination of selectivity of charge carriers, which would preferentially occupy lower bandgap phase, and the availability of efficient percolation pathways in the active layers.

These findings highlight the importance of the formulation of polymer-wrapped SWCNTs, bearing specific chiralities mixture, and of the control of the printing conditions of the networks on the overall device performances. We demonstrated that the polymer can play a role in sizing charge transport, as we verified holes relaxation onto it in high coverage networks. At the same time, we also found that optimal transport conditions, featuring vanishing thermal activation energy close to room temperature, suggesting the onset of a "band-like" transport regime and high field-effect mobilities, can be achieved in more sparse printed networks, even in presence of polymer strands wrapping the tubes. This is in agreement with the limited coverage of the nanotubes, granting their solubility but allowing high probability of nanotubes-to-nanotubes short contacts.[38]

Such knowledge is fundamental to devise future improvements of printed s-SWCNTs FETs with high, controlled and reproducible performances towards mass-produced, large-area and flexible electronic applications.

5. Experimental Section

Polymer Synthesis: Poly[4,4-didodecyl-*4H*-cyclopenta[2,1-b:3,4-b']-dithiophene-2,6-diyl)-alt-(2,1,3-benzothiadiazole-4,7-diyl)] (P12CPDTBT) has been synthesized by direct arylation polycondensation (DAP), following an already published procedure.[25–27] The synthesis was carried out in dry *N*,*N*-dimethylacetamide with palladium acetate as catalyst and potassium carbonate as base. After Soxhlet extraction with methanol, ethyl acetate, *n*-hexane and dichloromethane, the further used material was the higher molecular weight dichloromethane fraction of

P12CPDTBT with M_n = 11.500 g mol^{-1} and M_w = 57.200 g mol^{-1}. The batch showed relatively broad molecular weight distribution, typical for DAP products.

Ink Preparation and Characterization: HiPCO SWCNTs (0.8–1.2 nm) were purchased from Unidym Inc. The polymers were solubilized in toluene using a high power ultrasonicator (Misonix 3000) with cup horn bath (output power 69 W) for 10 minutes, followed by overnight stirring at 60 °C. Subsequently, SWCNTs were added to form the SWCNT:polymer dispersions with a weight ratio of 1:2 (3 mg of SWCNTs, 6mg of polymer, 15 mL of toluene). These solutions were then sonicated for 2 h at 69 W and 16 °C. After ultrasonication, the dispersions were centrifuged at 30 000 rpm (109 000 g) for 1 h in an ultracentrifuge (Beckman Coulter Optima XE-90;rotor: SW55Ti) to remove all the remaining bundles and heavy-weight impurities. After the centrifugation, the highest density components precipitate at the bottom of the centrifugation tube, while the low-density components, including small bundles and individualized SWCNTs wrapped by the polymer, and free polymer chains, stay in the upper part as supernatant. One extra step of ultracentrifugation was implemented to decrease the amount of free polymer in solution (enrichment).[40] For this purpose the supernatant obtained after the first ultracentrifugation, is centrifuged for 5 h, 55 000 rpm (367 000 g), the individualized s-SWCNTs were precipitated to form a pellet, and the free polymer was kept in the supernatant. Finally, the pellet was re-dispersed by sonication in oDCB. Optical measurements were performed to check the concentration of the carbon nanotubes selected by the polymers. Absorption spectra were recorded by a UV–vis–NIR spectrophotometer (Shimadzu UV-3600). The HiPCO:P12CPDTBT samples in oDCB had a concentration of 0.2 g L^{-1}.

Samples Fabrication: Low alkali 1737F Corning glasses were used as substrates for films and devices. Standard cleaning in Milli-Q water, acetone and isopropyl alcohol followed by O_2 plasma cleaning at 100 W were employed. The FETs were realized using a bottom-contact, top-gate geometry. Source and drain electrodes were patterned by a photolithographic process and deposited by evaporation of a 1.5 nm thick Cr adhesion layer and 15 nm Au film. Channel width is W = 200 µm, channel length L = 40 µm. The patterned substrates were then cleaned by ultrasonic bath in isopropyl alcohol for 3 min and exposed to O_2 plasma at 100 W for 5 min prior to printing of the nanotubes. The SWNT based ink was deposited as semiconducting layer with a custom inkjet printing system, Jetlab 4xI-A, provided with a nozzle orifice diameter of 60 µm. After the printing, the devices were annealed on a hotplate for 1 h at 150 °C in nitrogen atmosphere. A dielectric layer with thickness between 500–600 nm was obtained by spin-casting PMMA (Sigma-Aldrich) with M_w = 120 kg mol^{-1} from *n*-butyl acetate (80 g L^{-1}). After dielectric deposition, the samples were annealed in nitrogen at 80 °C for 30 min. The devices were then completed by thermally evaporating a 30 nm thick Al layer. For samples studied by CMS, the gate contact needed to be semi-transparent and therefore 7 nm of Al followed by 4 nm of Au were thermally evaporated.

Film Morphology Characterization: The surface topography of the films was measured with an Agilent 5500 Atomic Force Microscope operated in the Acoustic Mode.

Electrical Characterization: The electrical characteristics of transistors were measured in a nitrogen glovebox on a Wentworth Laboratories probe station with the aid of a Agilent B1500A semiconductor parameter analyzer. Temperature-dependent electrical characterizations were carried out in vacuum using a custom probe station system, in a temperature range between 200 and 300 K with a ΔT of 10 K for each step.

The mobility values in the linear and saturation regime were extracted using the gradual channel approximation, according to the parallel plate model. The mobilities reported to not take into account contact effects, that is, the data correspond to an effective mobility.

Charge Modulation Spectroscopy: CMS spectra were collected by measuring the normalized transmittance variation ($\Delta T/T$) induced by applying a modulated voltage. The measurements were performed in a vacuum chamber by keeping the source and drain electrode at 0 V, while the modulated voltage (f = 363 Hz) was applied at the gate electrode. The offset voltage and amplitude of modulation varied from sample to sample. Details on these values may be found in the figure captions. The probing light was obtained by monochromating a tungsten lamp source. Once monochromated, the light was focused on the device and then collected and revealed using a Si photodiode in the 500–1000 nm range (Thorlabs FDS100) and a InGaAs one (Thorlabs FGA21) in the 1000–1600 nm Near Infrared region. The electrical signal was amplified through a trans-impedance amplifier (Femto DHPCA-100) and then revealed using a DSP Lock-in amplifier (Standford Instrument SR830).

Supporting Information

Supporting Information is available from the Wiley Online Library or from the author.

Acknowledgements

The authors wish to acknowledge A. D. Scaccabarozzi and A. Perinot for support in several stages of the work and for fruitful discussions. This work was supported by the European Research Council (ERC) under the European Union's Horizon 2020 research and innovation program "HEROIC", grant agreement 638059. The microlithographic processes were carried out at Polifab, the micro-, and nanotechnology center of the Politecnico di Milano.

Conflict of Interest

The authors declare no conflict of interest.

Keywords

carbon nanotubes, charge transport, field-effect transistors, inkjet printing, thin film transistors

Received: August 14, 2020
Revised: October 15, 2020
Published online: October 27, 2020

[1] T. Dürkop, S. A. Getty, E. Cobas, M. S. Fuhrer, *Nano Lett.* **2004**, *4*, 35.
[2] G. J. Brady, A. J. Way, N. S. Safron, H. T. Evensen, P. Gopalan, M. S. Arnold, *Sci. Adv.* **2016**, *2*, e1601240.
[3] D.-M. Sun, M. Y. Timmermans, A. Kaskela, A. G. Nasibulin, S. Kishimoto, T. Mizutani, E. I. Kauppinen, Y. Ohno, *Nat. Commun.* **2013**, *4*, 2302.
[4] F. Xu, M.-Y. Wu, N. S. Safron, S. S. Roy, R. M. Jacobberger, D. J. Bindl, J.-H. Seo, T.-H. Chang, Z. Ma, M. S. Arnold, *Nano Lett.* **2014**, *14*, 682.
[5] D.-M. Sun, C. Liu, W.-C. Ren, H.-M. Cheng, *Adv. Electron. Mater.* **2016**, *2*, 1600229.
[6] W. Gomulya, G. D. Costanzo, E. J. F. De Carvalho, S. Z. Bisri, V. Derenskyi, M. Fritsch, N. Fröhlich, S. Allard, P. Gordiichuk, A. Herrmann, S. J. Marrink, M. C. Dos Santos, U. Scherf, M. A. Loi, *Adv. Mater.* **2013**, *25*, 2948.
[7] S. K. Samanta, M. Fritsch, U. Scherf, W. Gomulya, S. Z. Bisri, M. A. Loi, *Acc. Chem. Res.* **2014**, *47*, 2446.
[8] A. Graf, Y. Zakharko, S. P. Schießl, C. Backes, M. Pfohl, B. S. Flavel, J. Zaumseil, *Carbon N. Y.* **2016**, *105*, 593.

[9] V. Derenskyi, W. Gomulya, J. Gao, S. Z. Bisri, M. Pasini, Y.-L. Loo, M. A. Loi, *Appl. Phys. Lett.* **2018**, *112*, 072106.
[10] F. Yang, M. Wang, D. Zhang, J. Yang, M. Zheng, Y. Li, *Chem. Rev.* **2020**, *120*, 2693.
[11] W. Talsma, A. A. Sengrian, J. M. Salazar-Rios, H. Duim, M. Abdu-Aguye, S. Jung, S. Allard, U. Scherf, M. A. Loi, *Adv. Electron. Mater.* **2019**, *5*, 1900288.
[12] J. Zaumseil, *Semicond. Sci. Technol.* **2015**, *30*, 074001.
[13] V. Derenskyi, W. Gomulya, J. M. S. Rios, M. Fritsch, N. Fröhlich, S. Jung, S. Allard, S. Z. Bisri, P. Gordiichuk, A. Herrmann, U. Scherf, M. A. Loi, *Adv. Mater.* **2014**, *26*, 5969.
[14] S. G. Bucella, J. M. Salazar-Rios, V. Derenskyi, M. Fritsch, U. Scherf, M. A. Loi, M. Caironi, *Adv. Electron. Mater.* **2016**, *2*, 1600094.
[15] M. Brohmann, M. Rother, S. P. Schießl, E. Preis, S. Allard, U. Scherf, J. Zaumseil, *J. Phys. Chem. C* **2018**, *122*, 19886.
[16] J. Gao, Y.-L. L. Loo, *Adv. Funct. Mater.* **2015**, *25*, 105.
[17] S. Z. Bisri, V. Derenskyi, W. Gomulya, J. M. Salazar-Rios, M. Fritsch, N. Fröhlich, S. Jung, S. Allard, U. Scherf, M. A. Loi, *Adv. Electron. Mater.* **2016**, *2*, 1500222.
[18] M. Rother, S. P. Schießl, Y. Zakharko, F. Gannott, J. Zaumseil, *ACS Appl. Mater. Interfaces* **2016**, *8*, 5571.
[19] N. F. Zorn, F. Scuratti, F. J. Berger, A. Perinot, D. Heimfarth, M. Caironi, J. Zaumseil, *ACS Nano* **2020**, *14*, 2412.
[20] S. Kahmann, J. M. Salazar Rios, M. Zink, S. Allard, U. Scherf, M. C. Dos Santos, C. J. Brabec, M. A. Loi, *J. Phys. Chem. Lett.* **2017**, *8*, 5666.
[21] Y. Joo, G. J. Brady, C. Kanimozhi, J. Ko, M. J. Shea, M. T. Strand, M. S. Arnold, P. Gopalan, *ACS Appl. Mater. Interfaces* **2017**, *9*, 28859.
[22] T. Lei, X. Chen, G. Pitner, H.-S. P. Wong, Z. Bao, *J. Am. Chem. Soc.* **2016**, *138*, 802.
[23] J. M. Salazar-Rios, W. Talsma, V. Derenskyi, W. Gomulya, T. Keller, M. Fritsch, S. Kowalski, E. Preis, M. Wang, S. Allard, G. C. Bazan, U. Scherf, M. C. Dos Santos, M. A. Loi, *Small Methods* **2018**, *2*, 1700335.
[24] J. M. Salazar-Rios, W. Gomulya, V. Derenskyi, J. Yang, S. Z. Bisri, Z. Chen, A. Facchetti, M. A. Loi, *Adv. Electron. Mater.* **2015**, *1*, 1500074.
[25] S. Kowalski, S. Allard, U. Scherf, *ACS Macro Lett.* **2012**, *1*, 465.
[26] S. Kowalski, S. Allard, K. Zilberberg, T. Riedl, U. Scherf, *Prog. Polym. Sci.* **2013**, *38*, 1805.
[27] S. Kowalski, S. Allard, U. Scherf, *Macromol. Rapid Commun.* **2015**, *36*, 1061.
[28] H. Kataura, Y. Kumazawa, Y. Maniwa, I. Umezu, S. Suzuki, Y. Ohtsuka, Y. Achiba, *Synth. Met.* **1999**, *103*, 2555.
[29] J. H. Choi, M. S. Strano, *Appl. Phys. Lett.* **2007**, *90*, 223114.
[30] H. H.o Choi, K. Cho, C. D. Frisbie, H. Sirringhaus, V. Podzorov, *Nat. Mater.* **2018**, *17*, 2.
[31] C. Liu, T. Minari, Y. Xu, B.o-R.u Yang, H.-X. Chen, Q. Ke, X. Liu, H. C. Hsiao, C. Y.u Lee, Y.-Y. Noh, *Org. Electron.* **2015**, *27*, 253.
[32] M. Pope, C. E. Swenberg, *Electronic Processes in Organic Crystals and Polymers*, Oxford University Press, Oxford **1999**.
[33] W. Gomulya, J. Gao, M. A. Loi, *Eur. Phys. J. B* **2013**, *86*, 404.
[34] P. J. Brown, H. Sirringhaus, M. Harrison, M. Shkunov, R. H. Friend, *Phys. Rev. B – Condens. Matter Mater. Phys.* **2001**, *63*, 125204.
[35] Y. Tanaka, Y. Hirana, Y. Niidome, K. Kato, S. Saito, N. Nakashima, *Angew. Chemie – Int. Ed.* **2009**, *48*, 7655.
[36] M. Caironi, M. Bird, D. Fazzi, Z. Chen, R. Di Pietro, C. Newman, A. Facchetti, H. Sirringhaus, *Adv. Funct. Mater.* **2011**, *21*, 3371.
[37] X. Y.u Chin, G. Pace, C. Soci, M. Caironi, *J. Mater. Chem. C* **2017**, *5*, 754.
[38] R. A. Bell, M. C. Payne, A. A. Mostofi, *Phys. Rev. B* **2014**, *89*, 245426.
[39] H. W. Lee, Y. Yoon, S. Park, J. H. Oh, S. Hong, L. S. Liyanage, H. Wang, S. Morishita, N. Patil, Y. J. Park, J. J. Park, A. Spakowitz, G. Galli, F. Gygi, P. H.-S. Wong, J. B.-H. Tok, J. M. Kim, Z. Bao, *Nat. Commun.* **2011**, *2*, 541.
[40] S. Z. Bisri, J. Gao, V. Derenskyi, W. Gomulya, I. Iezhokin, P. Gordiichuk, A. Herrmann, M. A. Loi, *Adv. Mater.* **2012**, *24*, 6147.